Fabrication and Characterization of a Surface-Acoustic-Wave Biosensor in CMOS Technology for Cancer Biomarker Detection

Onur Tigli, *Member, IEEE*, Louis Bivona, Patricia Berg, and Mona E. Zaghloul, *Fellow, IEEE*

***Abstract*—Design, fabrication, and characterization of a novel surface acoustic wave (SAW) biosensor in complementary metal–oxide semiconductor (CMOS) technology are introduced. The biosensor employs a streptavidin/biotin-based five-layer immunoassay for detecting a prominent breast cancer biomarker, mammoglobin (hMAM). There is a growing demand to develop a sensitive and specific assay to detect biomarkers in serum that could be used in the early detection of breast cancer, determining prognosis and monitoring therapy. CMOS-SAW devices present a viable alternative to the existing biosensor technologies by providing higher sensitivity levels and better performance at low costs. Two architectures (circular and rectangular) were developed and respective tests were presented for performance comparison. The sensitivities of the devices were analyzed primarily based on center frequency shifts. A frequency sensitivity of 8.704 pg/Hz and a mass sensitivity of 2810.25 m^2/kg were obtained. Selectivity tests were carried out against bovine serum albumin. Experimental results indicate that it is possible to attach cancer biomarkers to functionalized CMOS-SAW sensor surfaces and selectively detect hMAM antigens with improved sensitivities, lowered costs, and increased repeatability of fabrication.**

***Index Terms*—Biosensor, cancer, complementary metal–oxide semiconductor (CMOS), microelectromechanical systems (MEMS), surface acoustic wave (SAW).**

I. Introduction

ACOUSTIC wave devices have been in commercial use for more than 60 years [1]. Although the telecommunications industry has been the primary employer of these devices, they are enjoying a large surge in several new emerging and developing industries. These industries constitute automotive, medical, and commercial applications. The vast majority of these industries use acoustic-wave devices as sensors. These sensors include but are not limited to torque, pressure, biological, chemical, temperature, vapor, humidity, and mass sensors. When compared to their competition, acoustic-wave sensors present a solid example of the effective use of acoustic-wave devices in diverse applications. They are versatile, highly sensitive, reliable, reusable, small, inexpensive, can easily be designed for responding to various measurands, have a wide dynamic range, and they are passive devices which can also be deployed as wireless units. Therefore, acoustic wave devices present attractive alternatives to their counterpart technologies in their corresponding sensor applications. The application of interest in this paper, namely, biosensor, presents a solid example of how effective acoustic-wave sensors can be used in diverse applications.

Surface acoustic waves (SAWs) are generated at the free surface of piezoelectric material. The application of a varying voltage to the metal interdigital transducer (IDT) generates the acoustic wave on the input side. The acoustic wave generated by the input IDT travels through the region called the delay line and reaches the output IDT where the mechanical displacements due to the acoustic waves create a voltage difference between the output IDT fingers. In order to employ mass loading on SAW sensors, the device surfaces should be functionalized by selective coatings that react with the entity under analysis. This interaction, while causing a mass loading, produces a shift in resonant frequency, which then can be measured to analyze the entity being sensed. The first examples of this approach came from the field of chemical sensors. Wohltjen and Dessy reported the first use of SAW devices for chemical analysis [2]. They laid out instrumentation design for chemical analysis, which uses SAW devices.

The principle of biosensors is very similar to the chemical vapor sensors that were listed in the literature. They detect targeted biological species in fluid or solid form by employing mass loading on acoustic-wave devices. This fundamental principle is depicted in Fig. 1 along with a typical frequency-shift-based response. The surface of these devices also requires a special coating to functionalize the sensors for the analytes of interest. Several techniques were developed and applied for a variety of analytes. These are DNA-RNA hybridization, adsorption of proteins on functionalized surfaces, lipid-protein interactions on membranes and piezoimmunosensing [3]. Due to the high specificity of antigen-antibody reactions and the well-structured generation of antibodies against a variety of biological materials made it possible to build immunosensors that employ acoustic-wave devices. The application example that is selected for this research is essentially a piezoimmunosensor that

Manuscript received February 12, 2009; revised May 18, 2009. First published December 04, 2009; current version published January 27, 2010.

An earlier version of this paper was presented at IEEE Sensors Conference 28-31 Oct. 2008 and was published in the conference proceedings.

O. Tigli is with Washington State University Vancouver, School of Engineering and Computer Science, Vancouver, WA 98686 USA (e-mail: tigli@wsu.edu).

L. Bivona and P. Berg are with the George Washington University, Biochemistry and Molecular Biology Department, Washington, DC 20052 USA (e-mail: lbivona@gwu.edu; bcmpeb@gwu.edu).

M. E. Zaghloul is with the George Washington University, Electrical and Computer Engineering Department, Washington, DC 20052 USA (e-mail: zaghloul@gwu.edu).

Color versions of one or more of the figures in this paper are available online at http://ieeexplore.ieee.org.

Digital Object Identifier 10.1109/TBCAS.2009.2033662

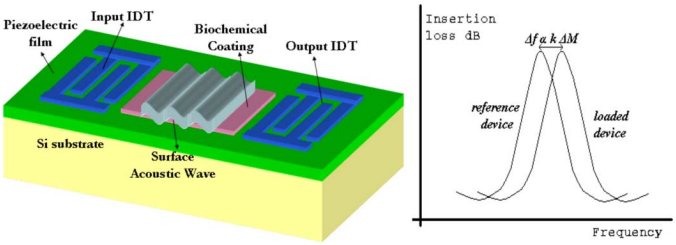

Fig. 1. Sketch of a typical SAW-based bio/chemical sensor using the mass loading principle. The center frequency shifts of the reference and the loaded devices are used to detect the change in the mass that is perturbing the SAW.

employs antigen-antibody binding to detect cancer biomarker mammoglobin (hMAM).

The applications of piezoelectric immunosensors are abundant and reported widely in literature. They include medical applications, such as bacteria, virus, and toxin detection [4], clinical diagnosis and analysis [5], as well as food industry and environmental analysis for the detection of compounds using antibody-antigen reactions [6]. Piezoelectric immunosensors for the detection of viruses and bacteria associated with acute diarrhea were reported in [7] with limits of 10^6 microorganisms/mL. Zhou *et al.* demonstrated the detection limits of 10^5/mL for hepatitis A and B viruses [8]. Immunoglobin M with detection limits of 5.5 cells/mL and insulin with a detection limit of 0.17 cells/mL were reported in [9] and [10], respectively. Cocaine detection with limits of 33 cells/mL and nicotine detection of 0.025 cells/mL were reported in [11] and [12], respectively. Other than the nicotine work, all of the listed biosensors work employed antigen-antibody binding as the assay principle. The nicotine work used molecularly imprinted polymer.

Although most of this initial piezoelectric immunosensor work was carried out by using (QCM) in the past, the increased sensitivities—primarily due to much higher operating frequencies—of SAW-based sensors attracted a lot of biosensor research interest and effectively replaced the use of QCMs over the years. Its integration possibilities with the current cutting-edge microelectromechanical systems–very-large-scale integrated (MEMS-VLSI) fabrication technologies and the production of higher sensitivities at lower overall costs made them a very attractive tool to exploit for biosensor applications. Ganske *et al.* demonstrated the use of SAW as an immunobiosensor for the detection of human interleukin-6 (IL-6) [13]. They reported IL-6 molecule concentrations of 15 pg/mL to 100 pg/mL with a frequency shift range of 4500 to 5700 Hz. Berkenpas *et al.* presented the use of a shear horizontal SAW biosensor on langasite substrates [14]. They used biotin-modified rabbit IgG and goat antirabbit IgG antibodies as the analyte and performed liquid medium experiments with phase change analysis. A more recent similar work that employed the same SAW substrate presented the detection of toxigenic E.Coli O157:H7 bacteria with phase responses of 14° compared to 2° anti-TNP (trinitrophenyl) binding [15]. Gizeli *et al.* carried out important investigations in liquid phase detection employing Love wave devices [16], [17]. Maximum sensitivity of 430 cm^2/g with a concentration range of 1 – 400 $\mu\mathrm{g}/\mathrm{ml}$ was reported for radiolabelled IgG adsorption [16]. As an example of vapor phase SAW biosensing, Stubbs *et al.* demonstrated the detection of uranine vapor on anti-FITC (fluorescein isothiocyanate)-coated SAW devices [39].

This paper introduces the biosensor application through an overview of the design fabrication and use of CMOS-SAW sensors along with a thorough comparison of rectangular and circular CMOS-SAW devices. After the completion of the proof-of-concept phase of this research, the CMOS-SAW devices were characterized thoroughly for performance [18]–[20]. Based on the results of this characterization, designs were improved for better performance. The following sections lay out the primary components of a biosensor system. Fabrication and characterization of these important components are laid out in detail. Sample results are presented for the experiments that were carried out for developing robust testing procedures, functionalizing gold-covered chips with streptavidin/biotin and antibody/antigen interactions. This paper concludes with the discussion of performance, and testing issues for the CMOS-SAW-based biosensors.

II. Biosensor Fundamentals

In essence, a biosensor can also be defined as an analytical device incorporating a biological sensing material with a transducer to detect and translate biological changes into known electrical signals. There are three significant components of a biosensor: 1) sensing material; 2) interface material; and 3) transducer. In order to successfully analyze the material under test, all of these components should be functioning effectively. There are several major factors that affect the performance of a biosensor. The sensing material determines the selectivity of the sensor. Therefore, this material should have high specificity and affinity to the molecules under analysis. The objective for this component is to produce a thin film of biologically active material on or near the transducer surface, which responds only to the presence of one or a group of materials requiring detection. The second component is the interface material. It provides a medium for the transducer to come into contact with the sensing materials by promoting direct contact and strong binding. In biosensor technologies, gold finds a wide use as an interface material. The third component in the system is the transducer. This component takes the most interest and determines the operational quality of the entire system, as it is the primary component that takes the chemical/biological interaction and converts it into electric signals.

III. Transducer Design

A. Mechanisms

There are several transducer mechanisms that are widely used for decades in various biosensor applications. These mechanisms and their corresponding methods can be summarized as [21]: electrochemical: potentiometry, amperometry, ISFET; electrical: surface conductivity, capacitance; thermal: calorimetry, enzyme thermistor; magnetic: paramagnetism;

optical: fluorescence, surface plasmon resonance, scattering; piezoelectric: QCM, SAW, SH/APM, Lamb wave, Love wave.

Each mechanism has their particular advantages/disadvantages and optimal applications. Several physical transducers are capable of measuring surface mass changes resulting from the biological materials at the sensitive area. Although mostly advanced optical systems are utilized, the piezoelectric and acoustic devices present similar but significantly less expensive alternatives [22]. As demonstrated in the literature, the adsorption of biomolecules on functionalized surfaces turned out to be one of the prominent applications of piezoelectric transducers. Examples of these applications include the interaction of DNA and RNA with complementary strands, specific recognition of protein-ligands by immobilized receptors, the detection of viruses, bacteria, and cells, as well as the development of immunosensors. Piezoelectric transducers enable a label-free detection of molecules. They are more than simple mass sensors since the sensor response is also influenced by interfacial phenomena, viscoelastic properties of the biomaterial, surface charges of adsorbed molecules, and surface roughness [23]. In this research, the transduction mechanism that was employed for the biosensor application is piezoelectricity.

Piezoelectric QCM has been the most widely used transduction for biosensor applications in the past several decades. However, there is an important advantage of SAW devices over the QCM. They can be designed to operate at higher frequencies and, therefore, the sensitivity of these devices to the same amount of analyte is increased remarkably. The other important limitation of the QCMs is that they use bulk acoustic waves and, consequently, result in reduced sensitivities than SAW devices which employ SAWs that are constantly in contact with the biomaterial. Recent advances in SAW device development and the unique features of the fabrication sequences that are developed for the CMOS-compatible SAW devices in our research prove that CMOS-SAW devices could replace the existing technologies being employed for biosensing by providing higher sensitivity levels and better performance.

B. CMOS-SAW Device Fabrication

The CMOS-SAW devices were fabricated in AMI Semiconductor's 0.5-μm 3-metal 2-poly technology [19], [20]. A three-step postprocessing sequence is applied to the CMOS finished dice. All three postprocessing steps are completely compatible with CMOS and do not disturb any of the CMOS layers. Fig. 2 presents the three-step postprocessing sequence. The postprocessing steps consist of: 1) reactive ion etch (RIE) for the IDT definition; 2) maskless ZnO RF magnetron sputtering for piezoelectric material deposition; and 3) pad frame definition through shadow mask photolithography. The details of these steps and the pertaining characterization data are detailed in our previous work [18]–[20]. CMOS-SAW devices employ design novelties, such as embedded heaters for temperature stability analysis, acoustic absorbers, and EM feedthrough contacts. Fig. 2(d) presents a finished CMOS-SAW die. One of the major challenges of the postprocessing sequence is to obtain highly oriented perpendicular sidewalls between the IDT fingers

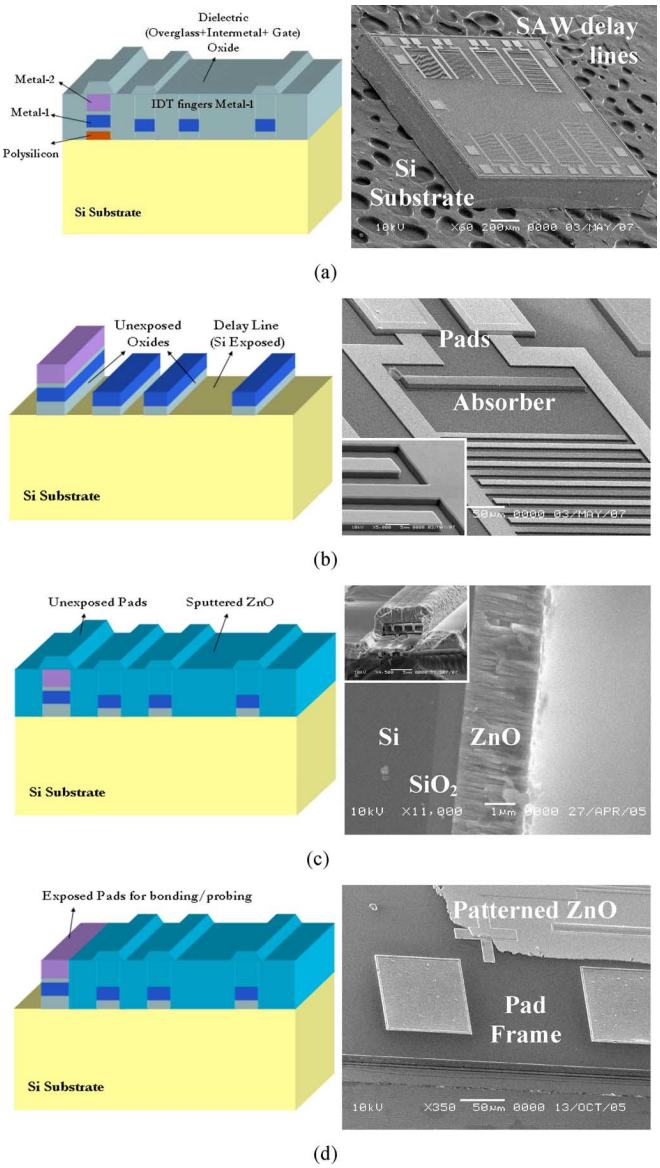

Fig. 2. Schematic depiction and SEM snapshots for (a) after CMOS fabrication, (b) oxide removal, (c) piezoelectric deposition, (d) and pad frame definition for the three-step postprocessing sequence.

for higher performance. This challenge was addressed by using RIE, which employs the top metal layers as masking for the underlying oxides. This step provided highly oriented IDT fingers without any loss of sidewall or connection metal integrity. Fig. 2(b) demonstrates the results of the RIE step. As can be observed from the figures, complete elimination of interfinger oxide layers was achieved. Fig. 2(b) also shows a closeup of a single IDT after the RIE step is completed. The acoustic absorber, pad connections, and IDT fingers are also displayed.

Another challenge was faced in the postprocessing sequence due to small-size die-level fabrication. After the zinc–oxide (ZnO) deposition, the entire die is covered with the sputtered ZnO. Fig. 2(c) shows the ZnO layer after the RF magnetron sputtering is completed. The detailed process parameters for the first three steps are reported in our previous work. In order to access the pads for bonding or probing purposes, a final step

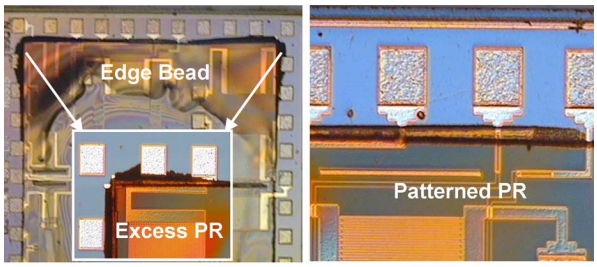

Fig. 3. (a) Top view of a typical CMOS-SAW die after photoresist development. Closeup of the pads after development showing excess PR (inset). (b) Closeup of the pad frame showing a well-defined edge masking.

TABLE I
PHOTOLITHOGRAPHY PROCESS PARAMETERS

Photoresist Step	Process Parameters				
	Prebake	Spin Speed	Spin Time	Exposure Time	Developer Time
Step 1	20 min. @ 100 °C	5000 rpm	40 sec.	20 sec.	120 sec.
Step 2	n/a	n/a	n/a	20 sec.	120 sec.

of patterning and etching is required. The typical die area is 1.5 mm × 1.5 mm and the custom designed pads are 100 μm× 100 μm. In order to carry out patterning and etching, the dice were mounted on microscopic glass slides to provide safe and easy handling. The major problem encountered during the patterning was the photoresist build up (edge bead) on the edges of the die. Due to the small size of the die, excessive amounts of photoresist were built up on the edges after spinning. This, in turn, created a nonuniform distribution of the photoresist on the areas where the pads are located. Thickness measurements showed a 2–4- μm PR buildup on the pad frame region when the thickness on the areas closer to the center of dies was measured to be 1 μm. The primary parameters that affect the build up are: 1) the spinner speed/acceleration; 2) the spin time; 3) the photoresist used; 4) the exposure time under the aligner, and, finally, 5) the time in the developer. After several experiments, these parameters were optimized for the process in hand. In order to completely remove the photoresist build up covering the pad frame, a two-step process was carried out. Table I summarizes the process parameters. In the first step, the dies were spun at 5000 r/min for a 40-s period. Then they were exposed for 20 s under UV light. A 5:1 (*DI Water: Developer*) developer was used for 120 s in the first step. Once this step was finished, the excessive photoresist due to build up is thinned down approximately to half its thickness. In the second step, the same exposure and development times were used to remove the photoresist on the edges completely. Microposit 351 Developer and Shipley 1818 photoresists were used. Fig. 3 shows the results of the photolithography steps. It is clearly seen in Fig. 3(a) that there is excess photoresist accumulation on the edges of the die close to the pad frame. This effect is considerably alleviated by using the two-step process as can be seen in Fig. 3(b).

IV. INTERFACE MATERIAL

Gold (Au) is virtually the only material that is being used in biomedical applications as the coating for transducers. This is mainly due to its outstanding material properties. It has outstanding resistance to tarnishing and corrosion, and has high electrical and thermal conductivity. It is easy to work with, and its high malleability and its amenability to plating in very thin films make it ideal for use in miniaturized components in electronics, medical, and other applications. Au is known for its resistance to corrosion, so it does not oxidize like other metals and it is chemically inert.

Au surfaces are very attractive candidates for self-assembly due to their metallic nature, great nobility, and particular affinity for sulphur. This aspect allows functionalization with thiols of various types and adhesion to diverse organic molecules, which are modified to contain a sulphur atom. These coatings, assembled onto the gold surfaces, can serve as biosensors [24]. This offers the prospect of preparing biomedical devices with interesting functionalities. Besides the highly useful material properties and its attractive features for biological compatibilities, gold provides additional advantages when used with SAW devices. The piezoelectric material being employed in this work, namely ZnO, shows a high binding to Au, which promotes effective isolation of the ZnO layer by reducing its reactive nature. Moreover, Au thin films on top of piezoelectric layers essentially provide very strong waveguiding. Au has a relatively low shear acoustic velocity and a high density when compared to the ZnO layer. Therefore, it presents a very effective waveguiding mechanism, which can be exploited for liquid phase sensing. Gizeli *et al.* reported the use of Au layers in a thickness range of 10 nm and 100 nm to investigate its effectiveness in shorting the electric field without interfering with the propagation of Love wave [25]. It was concluded that the Au layer does not reduce the viscoelastic acoustic wave interaction in the three-layered waveguide devices. Love wave devices present the most effective solution to the liquid phase-sensing problem of SAW devices as evidenced in various biosensor research in the literature [25]–[27]. The Love wave devices were shown theoretically and experimentally to be the most sensitive acoustic structure for liquid sensing. Therefore, using gold in this work also makes the potential liquid phase biosensor applications possible and provides improved sensitivity even for the solid phase application of the work presented here which employs dip and dry testing techniques. Due to all of these important features, Au was employed in this paper as the interface material between the biological sensing medium and the transducer.

For the biosensor application on the CMOS-SAW devices, additional postprocessing steps should be applied. After the fabrication steps that were detailed in Fig. 2 are completed, gold deposition and patterning should be carried out. Fig. 4(a) depicts the final step of gold deposition and the pertinent layers. As can be clearly seen from Fig. 4(b), the pad frame is patterned out completely and only the active sensor area is covered with the Au layer. Thermal evaporation is used for this purpose. The thermal evaporator employs resistive heating and very low pressures to sublimate Au. A high degree of vacuum is achieved

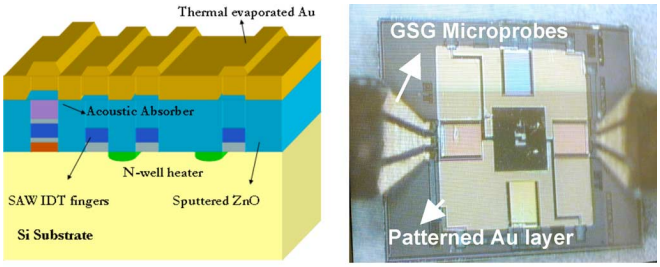

(a) (b)

Fig. 4. (a) Postprocessed biosensor layers after Au evaporation. (b) Snapshot that shows the GSG-configured probe tips in contact with the pads of a CMOS-SAW biosensor that is patterned for an active gold surface.

through a combination of a mechanical roughing pump and a high-vacuum pump. Airco Temescal CV-8 power supply with a 130-V input was used to apply current through the boat. The chamber pressure of 1.1×10^{-6} Torr was set and monitored with an ion gauge. The thickness of the Au is aimed to be 1000 Å. A deposition rate of 330 Å/min was attained for the samples. Multiple samples were deposited simultaneously to provide uniformity and repeatability between the samples.

Once the Au deposition is finalized, the samples were taken through the patterning process. This process followed the same mask and lithography that was detailed in [20] for the ZnO layer. As for the final step of etching, Metex auto strip gold etchant solution was used. This etchant offers a highly selective etch at a temperature range of 50–60 °C. The samples were etched at an average temperature of 55 °C in two steps to control the etch rate. A total of a 1000-Å-thick Au layer was etched completely in 1 min and 25 s which translates into an etch rate of 11.76 Å/min.

Since the quality of the Au thin films plays a crucial role in the overall sensitivity of the devices, thorough characterization is required. As in the case of the ZnO piezoelectric layer, the surface morphology, surface roughness, and the crystal orientation/structure are the subject of interest. To address these interests, optical microscopy, X-ray diffraction (XRD), and atomic-force microscopy (AFM) analyses were carried out. For comparative analysis, $2\theta_i$ scans of a dummy die (Au-Si) and a patterned die (Au-ZnO-SiO_2-Si) were carried out. As can be seen from Fig. 5(a), the Au film shows its peak at $2\theta_i = 38.921$, which agrees with the tabulated data in the literature [38]. The same peak is also obtained in the case of the patterned die. However, due to highly expressed perpendicular ZnO crystallography, the gold peak is suppressed in comparison. Fig. 5(b) shows the XRD curve obtained for this case. As demonstrated in this curve, the ZnO (002) peak at $2\theta_i = 34.84$ presents much higher intensity than the Au peak. This is expected due to the highly perpendicular c-axis orientation of ZnO. Multiple layers cause the intensity values to vary when compared to a single layer. The ratio of Au to ZnO thickness is 1/30, which results in overexpression of ZnO peaks in this XRD curve.

Surface roughness plays an important role in the overall functionality of the gold surface for biosensor applications. Perfectly smooth surfaces with the lowest possible grain sizes are desirable to promote strong binding and effective immobilization on the Au thin films. In order to analyze the quality of the Au surface after evaporation, AFM analyses were carried out. Fig. 6 presents the results for the surface roughness and grain size analyses. As shown in the surface roughness profile of the surface in Fig. 6(c), the Au surface presents an average grain size of 3.66 nm with a maximum of 6.63 nm and a minimum of 1.23 nm. As evidenced by these figures, the thermally evaporated Au thin-film surface shows an extremely smooth surface with very low grain sizes. This aspect plays an important role in defining and applying the immobilization technique.

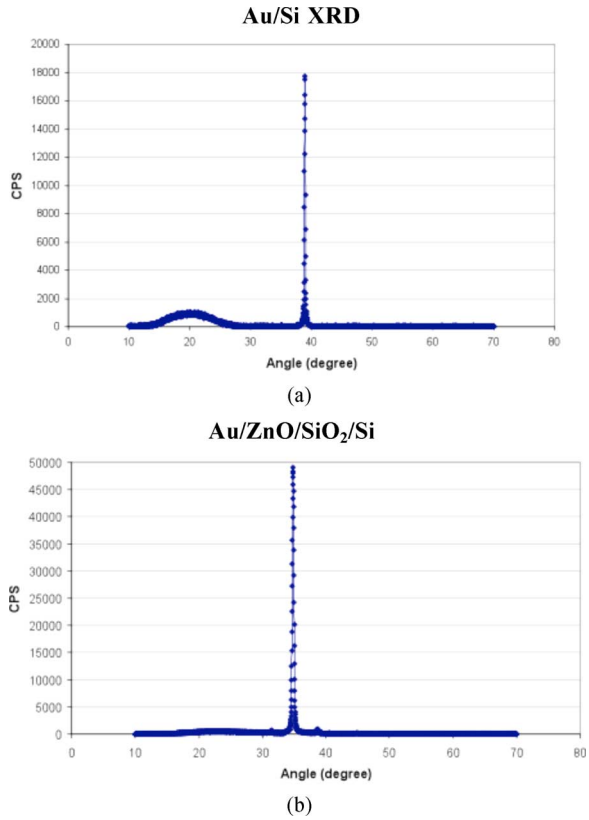

Fig. 5. (a) XRD curve for the Au thin film on an Si dummy chip. Note the peak $2\theta_i = 38.921$ for Au. (b) XRD curve for the Au thin film on the ZnO/SiO_2/Si chip. Note the much higher peak value of ZnO crystal (002) at $2\theta_i = 34.84$ suppressing the Au peak.

V. Biological Sensing Material

Piezoelectric immunosensors are accepted to be one of the most sensitive analytical instruments, being capable of detecting antigens in the picogram range [28]. Moreover, they have the potential to detect antigens in the gas phase as well as in the liquid phase. In order to achieve this sort of high sensitivity, the sensing material of the biosensor system plays a very important role. There are several conditions that must be satisfied for such a system [21]: 1) the biological component must retain substantial biological activity when attached to the sensor surface; 2) the biological film must remain associated with the sensor surface while retaining its structure and function; 3) the immobilized biological film needs to have long-term stability and durability; and 4) the biological material needs to have a high degree

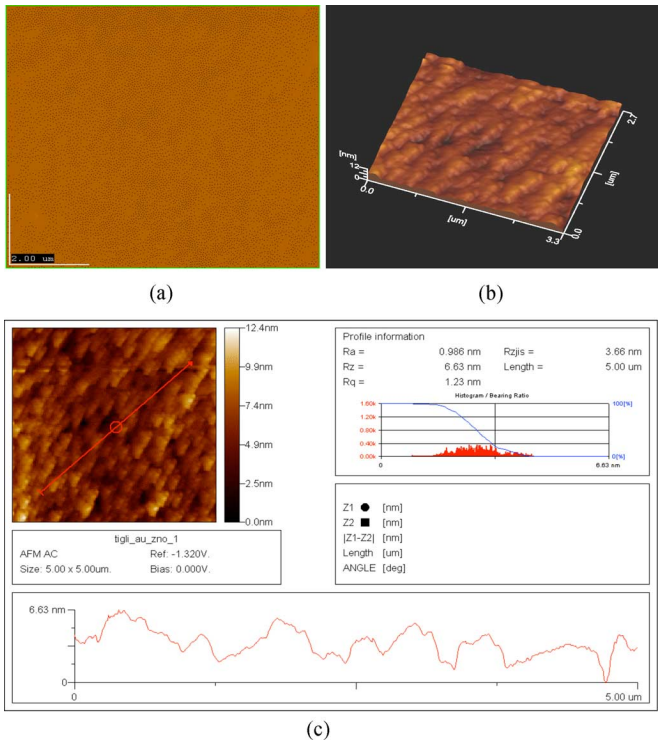

Fig. 6. (a) AFM raw snapshot taken for a 5 μm× 5-μm area showing a uniform smooth Au surface. (b) 3-D rendering of a 3 μm× 2.7-μm closeup of the Au surface showing the grain sizes smaller than 10 nm. (c) Profile distribution of the surface showing an average grain size of 3.66 nm.

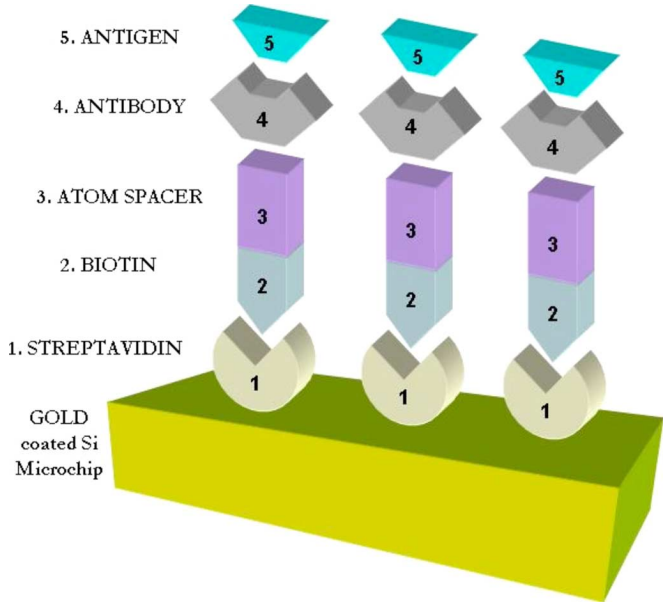

Fig. 7. Conceptual representation of the biosensor-sensing material assay. The antigen of interest in this study is hMAM, a secreted protein associated with breast cancer.

of specificity to a particular biological component. Once these conditions are met, the most important step for affinity-based biosensors is to apply an effective immobilization technique to provide the desired distribution and orientation of biomolecules.

The adsorption of biomolecules from the solution onto solid surfaces can proceed via either physical or chemical interactions. In early work, immobilization by adsorption was used successfully to couple proteins to various solid substrates [29]. More recent work has focused on the binding of biomolecules onto metal surfaces for biosensing applications [30]. Despite the intense research into biomolecule immobilization techniques, no generally applicable method has yet been developed. The primary techniques that are being used are: 1) adsorption; 2) immunoglobin-binding proteins (protein G, protein A); 3) avidin/biotin; and 4) dextran. According to the detailed study by Mascini *et al.* [31], dextran and avidin/biotin are found to be the best methods for the immobilization of biomolecules on piezoelectric transducer surfaces. These methods were found to be the most effective due to their high surface density of functional molecules, controlled distribution and orientation, absence of nonspecific binding, and the possibility of regeneration. For the biosensor application in our work, the avidin/biotin immobilization technique was selected and applied. As for the analyte of interest, mammoglobin (hMAM), a secreted protein associated with breast cancer, was selected. Fig. 7 depicts the conceptual representation of the biosensor-sensing material assay with the pertinent layers of bound molecules.

hMAM expression is specific for breast carcinoma, with infrequent expression in uterine carcinoma [32]. Immunohistochemical (IHC) staining demonstrated hMAM expression in 72% of primary breast tumors [32]. By quantitative RT-PCR, more than 90% of tumors were hMAM positive, and there was a correlation between hMAM expression and estrogen receptor (ER)-positive tumors [33]. Examination of blood from breast cancer patients links hMAM expression with metastasis [34]. Recently, an ELISA was developed to measure hMAM in sera; the sera from all 26 women with metastatic breast cancer was hMAM positive [32]. From all of these recent works, it was concluded that hMAM is a new serum biomarker with utility in the early detection of recurrence and as an indicator of treatment response. Due to this experimentally proven importance and relevance in cancer research, hMAM was picked as the antigen of interest in our biosensor application. It is clear that increasing the sensitivity of assays for serum biomarkers, such as hMAM, would be advantageous and allow their use in early detection as well as diagnosis.

Proteins can be immobilized onto gold surfaces via thiol groups in a thiolation reaction [35]. Thiolation is achieved by converting the intrinsic amines found in proteins into thiol groups, which bind readily with metal surfaces, such as gold [35]. Fluorophore-conjugated streptavidin was thiolated and immobilized onto the gold surface of the sensors. The primary goal of this step is to attain the highest possible surface coverage by the streptavidin molecules. Alexa Fluor 405 conjugate of streptavidin was used and then visualized by using the Olympus BX-60 Microscope with the Image-Pro Plus Software. Fig. 8 displays the representative images of sequential overnight streptavidin applications at room temperature with 9.5 μM Alexa Fluor 405 Streptavidin, followed by washing in PBS/0.05% Tween. As can be seen from the figure,

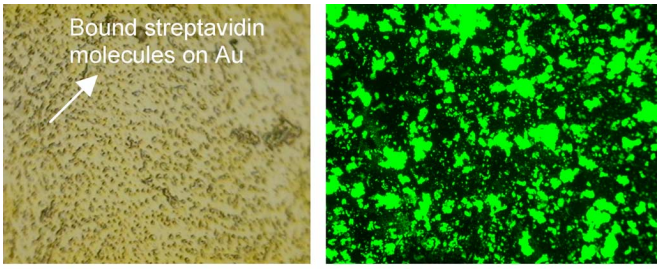

Fig. 8. (a) Optical microscopy snapshot of the sensor surface with streptavidin binding. (b) Fluorescent microscopy snapshot showing a surface coverage efficiency of 80%–90%.

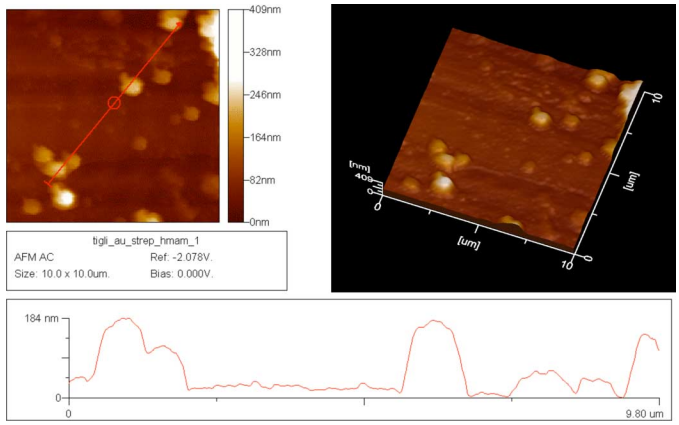

Fig. 9. AFM profile measurements and 3-D visualization for streptavidin-coated Au. The maximum streptavidin molecule size is measured to be 184 nm.

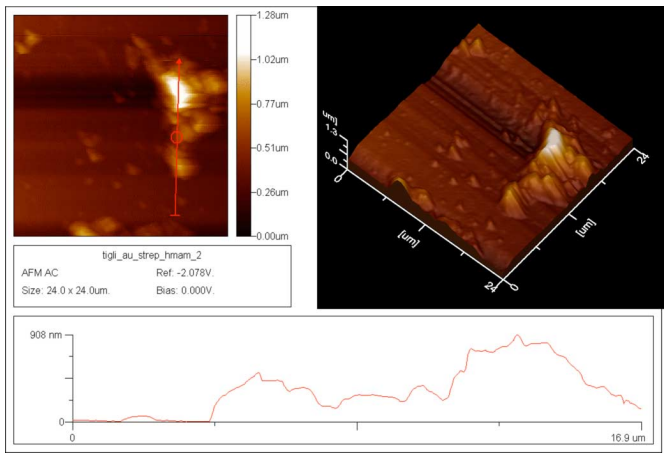

Fig. 10. AFM profile measurements and 3-D visualization of the Au sensor surface after hMAM Ab binding. An antibody molecule size of 906 nm is measured.

80%–90% of the gold surfaces of the sensors are coated with streptavidin. In order to visualize the streptavidin binding on the CMOS-SAW chip surfaces, optical microscopy was also used in the experiments. Fig. 8(a) shows the resulting snapshots from the streptavidin-covered gold sensor surface. The next step is the biotinylation of hMAM Ab and immobilization onto the streptavidin surface. A rabbit polyclonal Ab against hMAM (Abcam) was used for biotinylation with the biotin. The biotinylated Ab was incubated with the streptavidin-coated surface of the biosensor for 30 min. to 1 h for immobilization, and unbound biotinylated Ab was removed with several washes with PBS, pH 7.4. After the immobilization of the hMAM Ab is completed, the binding is also confirmed by using the optical and fluorescence microscopy. Both of these methods provide quantification information. However, it is also desirable to visualize the binding by comparing size and shapes of the molecules. For this purpose, detailed AFM analyses were carried out on the samples, which revealed relative size and binding information. Figs. 9 and 10 present the AFM results for streptavidin only and hMAM Ab, respectively. Discrete streptavidin molecules with an average size of 184 nm can be clearly observed on the Au surface in Fig. 9. The profile measurements in Fig. 10 show a large hMAM Ab island of size 908 nm. Careful investigation also shows the relatively smaller streptavidin molecules scattered around the Au surface. The results demonstrate that a successful immobilization technique is applied and resulted in high-efficiency functionalization of the Au surfaces. Moreover, a strong antibody-antigen interaction is attained with the recognition of hMAM protein by the antibody.

VI. Results and Discussion

The typical performance characteristics of interest for SAW devices are the insertion loss, center frequency, and their respective behavior against various measurands. As a secondary performance metric, phase responses are also used. In order to obtain these performance metrics, a wide spectrum, high-accuracy radio-frequency (RF) network analyzer is required. In addition to this requirement, the overall testing setup should accommodate direct electrical access to the devices in hand. The regular microchip-packaging techniques provide overall device stability and elimination of certain losses due to ambient variations. However, they only provide fixed electrical contacts, which hinder the micron-level physical-access flexibilities offered by electrical probing techniques. Besides these flexibilities, probing techniques also offer robust, and reproducible multiple experiments without compromising device integrity. They also provide direct contact to the actual contact pads, which eliminates the losses due to the bonding wires, package fingers, external circuit wiring, and board connections. Therefore, micron-level RF electrical probing was used to characterize the CMOS-SAW devices. The Cascade Microtech, Inc. [36] probe station was utilized for the experiments. This station utilizes two probes mounted on fixed locations. It is also integrated with an Olympus SZ60 microscope and Javelin chromachip V CCTV camera for high-precision probing and sample monitoring. As for the network analyzer, the HP 8712ET, 300 kHz–1300 MHz, RF network analyzer was used. This instrument integrates an RF synthesized source, transmission/reflection testset, multimode receivers, and display. The source features 1-Hz resolution, 40-ms sweep time, and up to +16-dBm output power [37]. The network analyzer is

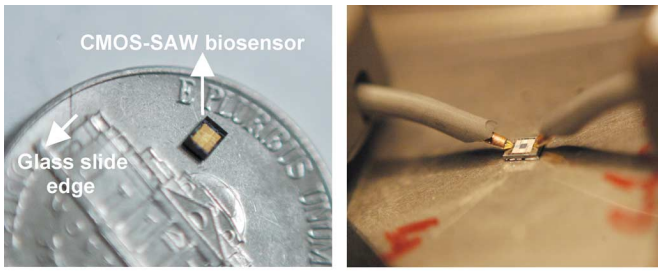

(a) (b)

Fig. 11. (a) Typical CMOS-SAW biosensor die on a nickle. (b) Snapshot showing the GSG-configured probe tips in contact with the pads.

connected to the probes via 40-GHz, 48-in-long microwave coaxial cables.

Air coplanar probes (ACP-40) from Cascade Microtech are used for probing experiments. These probes have a maximum specified frequency of 40 GHz and they employ 2.92-mm connectors with standard tips of berrylium/copper. For the experiments, a ground-signal-ground (GSG) probe configuration is used. In this configuration, three probe tips are aligned with a center-to-center distance of 100 μm. This probe configuration inherently dictated the contact pad design of the devices. In the case of CMOS-SAW devices, the G contact pads are shorted with on-chip metal routing to act like a single pad. This pad is then connected to the substrate contacts to provide the necessary electromagnetic (EM) feedthrough suppression by grounding the substrate. The pads are 100 μm$\times$ 100 μm in size and centered around the S pad with a 100-μm pad-to-pad distance. Fig. 11(b) shows the probe tips when they are in contact with the on-chip pads. The device in this snapshot is a completed biosensor device with the patterned gold surface before any biological coating is applied.

A. Electrical Characterization

In order to attain accurate and reproducible characterization results, precise measurement calibration is required. For the CMOS-SAW measurements, a 50 Ω-load standard calibration substrate was used. The analyzer offers four types of calibration choices for the transmission characteristics: 1) default response; 2) response; 3) response and isolation; 4) enhanced response. All four methods were conducted and compared for the experimental results. The third and fourth methods were found to offer the most accurate and stable results. This is explained by the fact that they are the only two methods that employ actual load calibration on both ports. Moreover, they offer superior calibration for the removal of systematic errors caused by frequency response, source match, and crosstalk, which are the most probable issues with the CMOS-SAW device measurement setups. Although these standard calibration methods provide compensation for the test setup-related issues surrounding the design under test (DUT), they do not address any probe irregularities. In order to compensate for these or any additional irregularities due to the micron-level probe-tip interactions, a special calibration kit (Cal-kit A or B) that was developed specifically for the GSG probes was used. Thorough electrical characterization was carried out and detailed results were presented in our previous work [18]–[20].

As laid out in these papers, transfer characteristics of two types of CMOS-SAW devices were attained, namely: 1) rectangular and 2) circular. The circular CMOS-SAW device was introduced as a design novelty for improved SAW performance [20]. Performance metrics comparison of these devices was reported in our previous work. As a continuation of this comparative analysis for sensor applications, both types of devices were subjected to the same biosensor experiments in this research.

B. Biosensor Application Experiments

In order to carry out the experiments for the biosensor application, additional test procedures and testing equipment were developed. These additional efforts include a thin glass handling substrate for easy handling of the small-size CMOS-SAW dice and a six-well plate test bench for biological fluid delivery on the chips. A regular six-well plate was machined to accommodate micropipette tips. Fig. 11(a) shows a typical CMOS-SAW biosensor die placed on a thin glass microscope slide. The glass slides provide easy handling of the dice during postprocessing and biosensor experiments. The dice are mounted on the slides by heating the substrates and applying wax on the backside. The wax provides robust sticking and is not affected by any of the chemicals that were applied during the postprocessing or the biological experiments. The six-well plate cells offer sufficient volume for dipping, rocking, and direct delivery of biological fluids on the chips.

The testing to reveal sensitivity and selectivity of the biosensors start with the functionalization of the gold surfaces. This is initiated by the application of streptavidin. Streptavidin was dissolved to make a 1-mg/ml solution in H_2O. After thiolating the streptavidin, 3.2 μl of thiolated streptavidin was applied in four steps of 0.8 μl. Streptavidin binding essentially sets up the foundation for more target molecules to be detected. Therefore, it is desirable to increase streptavidin surface coverage by adding more solution. Multiple applications also offer information on determining the saturation of the sensor surface. Each application was followed by an evaporation of the additional solution and a wash in 1 $\times$ PBS with slow rocking for 10 min. This was then followed with two washes with DEPC water to remove any unwanted ions from the active sensor surface and contact pads. Small amounts of ion buildup occurred on the pad regions of rectangular devices. On the other hand, circular devices performed much better in holding the solution intact on the effective sensor surface without any excess spill to the surrounding pad frame. Measurements were taken for each application. The transfer characteristics were analyzed, and a relationship was obtained between the application of streptavidin and the center frequency shifts. Fig. 12(a) presents the transfer function before and after the streptavidin applications. A frequency shift of 312.5 kHz was obtained for this experiment. For the maximum value tracking, the measurements were taken for each step of the experiments with multiple readings. This was achieved by reducing the frequency step precision to its lowest possible value (i.e., 1 Hz) focusing the sweep on the peak value range of the response 1 MHz. In order to observe any possible variation due to

frequency sweep within this low range of frequency, multiple snapshots were taken over time for the same measurements. These multiple readings were averaged to obtain the exact value representing a particular peak reading. The highest variation in these readings was $+/-1-8$ Hz, which translated into 1–8 ppm (assuming a 1-MHz range). Relative frequency shifts for each application are also a point of interest to gain insight into sensitivity and saturation. The relative frequency shifts versus the streptavidin application step are plotted in Fig. 12(b). *Device-1* and *Device-2* represent the circular and rectangular devices, respectively. Both results demonstrate very similar trends in frequency shifts by each application. It is important to note that the experiments were conducted under the same conditions for both devices. The circular device shows slightly larger shifts when compared to the rectangular devices. However, this is not sufficient evidence to conclude that the sensitivity of the circular device is better. The relatively larger shifts might be simply attributed to the improved effective binding of streptavidin on the circular sensor area. Although the same amounts of solutions were used for both types of devices, it was observed that the applied solution would stay intact in a bead shape on top of the circular device during the evaporation cycle whereas for the rectangular device, it would rapidly disperse over the entire die area, including the nonactive sensor regions.

In general, the sensitivity for acoustic-wave sensors is defined as the relative change in frequency due to mass loading divided by the surface density of the deposited mass [16]. By separating the two primary components in this definition, one can obtain two different figures of performance, namely, the frequency sensitivity and mass sensitivity. For frequency sensitivity, the $\Delta m/\Delta f$ expression is calculated for the devices and found to be 8.704 pg/Hz and 12.495 pg/Hz for the circular and rectangular devices, respectively. This value scales well with similar work in the literature. Stubbs *et al.* reported 0.232-pg/Hz sensitivity levels for a SAW-based vapor-phase biosensor to detect uranine vapor [39]. CMOS-SAW devices present much better mass sensitivities when compared to the same work. For the mass sensitivity figure, the $A/\Delta m$ expression was used and for CMOS-SAW, it was found to be 2810. 25 m^2/kg whereas the devices reported in [39] were calculated to be 3.58 m^2/kg. This calculation assumes the maximum amount of protein (1.8 mg) being attached to the surface and the device dimensions as reported by the authors [39]. CMOS-SAW devices scale better in this calculation due to the much smaller device dimensions and the ability to detect smaller masses on the same unit areas. McHale *et al.* reported a theoretical sensitivity value of 1750 m^2/kg for a love wave device when PMMA was used as the guiding layer []. CMOS-SAW figures compare well to this theoretical study as well. Note that for CMOS-SAW, in both sensitivity calculations, approximately 85% efficiency was assumed for surface coverage by streptavidin binding sites. This assumption is based on the surface coverage tests conducted for streptavidin as laid out in the previous sections. An average surface coverage of 80%–90% was observed by optical and fluorescence microscopy.

Once the streptavidin is attached to the sensor surfaces, the next step was to test the hMAM recognition by the sensors. For this step, 6 μl of biotinylated antihuman mammaglobin antibody (Ab) was added to 2 ml of PBS/%5 milk/0.05% TWEEN solution. This solution amounts to a final concentration of 0.0015 $\mu g/\mu l$ which results in a 3-μg total hMAM Ab. Due to the amount of the required solution, it is not practically possible to use pipette tips to deliver them on the chips. Therefore, the dip and dry method is used. This method requires the sensors to be placed in six-well plate cells and then immersed into the prepared Ab solutions. The plates are then incubated in a cold room for 2.5 h followed by PBS and DEPC water washes. As a final step, 2 ml of hMAM in buffer solution was prepared with an hMAM concentration of 0.1 $\mu g/\mu l$. The sensors are immersed into this solution in the same manner as the hMAM Ab. The devices are incubated overnight after hMAM applications. The transfer characteristics measurements are taken for each step of these experiments. Fig. 13 presents the resulting center frequency-shift curves for the rectangular devices. The rectangular CMOS-SAW designs contain two delay lines on the same chip. Therefore, there is the possibility of taking two separate measurements from the same chip. The dashed line represents the first delay line and the solid line shows the response measured from the second delay line. They follow each other very closely for the first four experiment steps as expected. It is important to

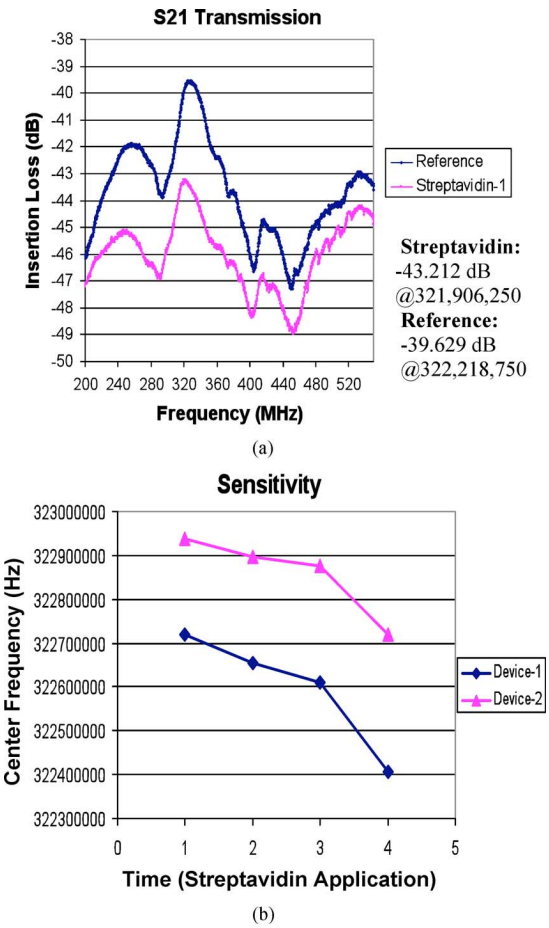

Fig. 12. (a) S_{21} transmission curves for the reference device before and after the application of streptavidin. (b) Center frequency shifts for the four-step streptavidin application. The x-axis represents the experiment step number for the streptavidin application.

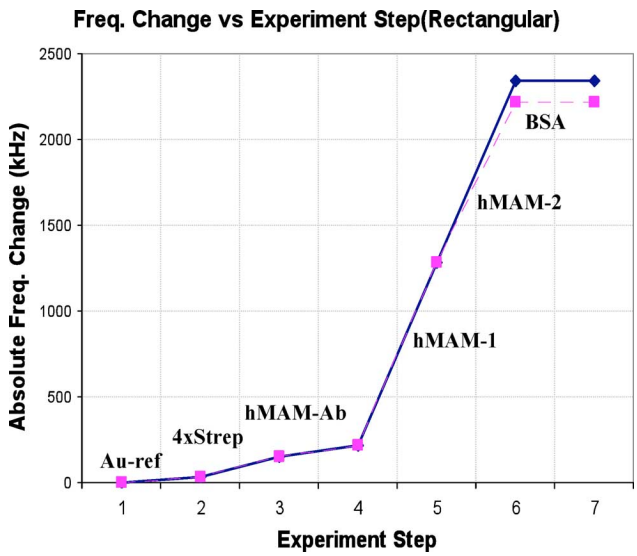

Fig. 13. Overall biosensor response to each set of applied materials. The frequency-shift axis shows absolute changes. Each marked interval represents an application for one of the biosensor elements.

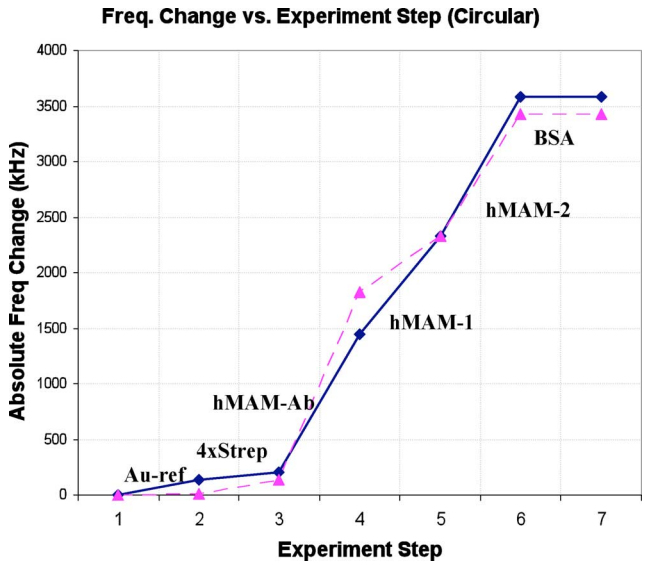

Fig. 14. Overall frequency change response of circular CMOS-SAW devices. The dashed line represents the first access point readings and the solid line shows the data collected from the second access point on the same chip.

note that the frequency shift axes for both cases are plotted for an absolute change in frequency Δf as opposed to the actual negative shifts. Another important observation from the figure is that the Ab gives a shift that is in the same range as the streptavidin. This was expected as the total amount of applied streptavidin mass is slightly larger (0.2 μg) than the hMAM Ab-applied mass.

A very similar overall response was obtained for the circular device. Fig. 14 presents the results in the same fashion. It is observed that the circular device presents a much higher frequency shift for the Ab binding. The rest of the experiments yielded in frequency shifts of the same ranges. This observation inherently suggests that the Ab surface coverage was much higher for the circular devices. This result is also verified by visual analysis of the coverage on both chips. In the case of the circular CMOS-SAW biosensor, the streptavidin and hMAM Ab binding sites are highly concentrated on the effective sensing area, which is defined by the delay line path. However, for the rectangular devices, although the amounts of applied materials were kept the same, the actual binding on the sensor surface is highly dispersed. This argument is supported by the high magnification optical microscope snapshots for both cases. Fig. 15 demonstrates the snapshots of the effective sensor areas with the binding sites. Concentrated binding sites on the circular device delay-line path are clearly observed. The figures also reveal that the access to the contact pads is preserved better for the case of circular devices.

In order to demonstrate the selectivity of the CMOS-SAW biosensors, a final set of experiments was conducted. For selective measurements against hMAM, a competitor protein, namely, bovine serum albumin (BSA) was used. hMAM-covered biosensors were immersed in BSA solutions with concentrations $10\times$ higher than hMAM. The same wash and incubation procedures were applied. The measurements after the BSA application did not show any significant frequency shift which is reflected in Figs. 13 and 14 as the final experiment step. This proves that the hMAM Ab layer is selectively detecting hMAM protein and not binding to BSA.

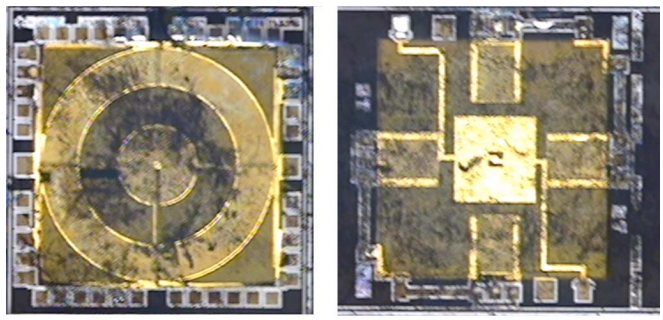

(a) (b)

Fig. 15. (a) Postprocessed biosensor layers after Au evaporation. (b) Snapshot that shows the GSG-configured probe tips in contact with the pads of a CMOS-SAW biosensor that is patterned for the active gold surface.

VII. Conclusion

The CMOS-SAW devices are generic sensor systems that can be employed in various forms of sensor applications with minimum effort. As a proof of concept for sensor applications, the use of CMOS-SAW devices as a biosensor proved to be a viable alternative to currently available piezoimmunosensors. A comprehensive investigation of biological interactions and their integration to the readily available CMOS-SAW devices were carried out. The preliminary studies and pertaining experiments resulted in selective detection of a prominent cancer biomarker, hMAM. The sensitivity figures agreed closely with the theoretical calculations that were carried out for comparison. However, with an experimentally documented high-temperature coefficient of delay [38], the limitations imposed by the dry fashion testing and the testing equipment incurred errors and contributed negatively in the overall performance of the sensors.

This yielded in at least one degree higher shifts when compared to similar work that employs SAW devices [14]–[16], [39]. Further investigation of the electrical properties of the biological materials that were used can potentially provide a method to decouple the impedance-related errors. Although overexpressed for certain experiments, the biosensor yielded selective detection of all the added biomaterials, including the protein of interest hMAM with a relatively easy procedure. Therefore, it can be concluded that the broad objective to design, model, fabricate, postprocess, and characterize SAW devices in CMOS technology for biosensor applications was fulfilled. These devices yielded mass sensitivities of 8.704 pg/Hz and 80%–90% streptavidin attachment efficiencies.

ACKNOWLEDGMENT

The authors would like to thank Prof. G. Harris for allowing them to use the facilities as well as J. Griffin and Dr. Z. Peizhen for the invaluable technical support in completing SEM and AFM characterization. The authors would also like to thank Dr. B. Thibeault for the RIE and Dr. G. Book for the RF sputtering work. The postprocessing steps were carried out at The Howard University Nanoscale Science and Engineering Facility.

REFERENCES

[1] B. Drafts, "Acoustic wave technology sensors," *IEEE Trans. Microw. Theory Tech.*, vol. 49, no. 4, pp. 795–802, Apr. 2001.
[2] H. Wohltjen and R. Dessy, "Surface acoustic wave probe for chemical analysis I: Introduction and instrument design," *Anal. Chem.*, vol. 51, no. 9, pp. 1458–1475, 1979.
[3] A. Janshoff, H. J. Galla, and C. Steinem, "Piezoelectric mass-sensing devices as biosensors- An alternative to optical biosensors?," *Angew. Chem. Int. Ed.*, vol. 39, pp. 4004–4032, 2000.
[4] R. M. Carter, J. J. Mekalanos, M. B. Jacobs, G. J. Lubrano, and G. G. Guibault, "Quartz crystal microbalance detection of Vibrio cholerae O139 serotype," *J. Immunol. Meth.*, vol. 187, pp. 121–125, 1995.
[5] S. Drost, S. Hauck, E. Yacoub-George, H. Wolf, S. Koch, C. Koßlinger, B. Hillerich, and K. Hieber, "Application of bioactive layers for chemical sensors and analysis systems," *Mater. Sci. Forum*, vol. 287-288, pp. 521–524, 1998.
[6] R. Blonder, S. Levi, G. Tao, I. Ben-Dov, and I. Willner, "The enhancement effect of gold nanoparticles as a surface modifier on DNA sensor sensitivity," *J. Amer. Chem. Soc.*, vol. 119, pp. 10467–10478, 1997.
[7] B. Konig and M. Gratzel, "Detection of viruses and bacteria with piezoimmunosensors," *Anal. Lett.*, vol. 26, pp. 1567–1575, 1993.
[8] X. D. Zhou, L. J. Liu, M. Hu, L. L. Wang, and J. M. Hu, "Detection of hepatitis B virus by piezoelectric biosensor," *J. Pharm. Biomed. Anal.*, vol. 27, pp. 341–345, 2002.
[9] M. R. T. C. Tan, C. X. Chu, G. L. Shen, F. Y. Xie, and R. Q. Yu, "Piezoelectric immunoassay for the detection of human serum albumin," *Anal. Lett.*, vol. 30, pp. 1783–1796, 1997.
[10] S. Saha, M. Raje, and C. R. Suri, "Sandwich microgravimetric immunoassay: Sensitive and specific detection of low molecular weight analytes using piezoelectric quartz crystal," *Biotechnol. Lett.*, vol. 24, pp. 711–716, 2002.
[11] B. S. Attili and A. A. Suleiman, "A piezoelectric immunosensor for the detection of cocaine," *Microchem. J.*, vol. 54, pp. 174–179, 1996.
[12] Y. G. Tan, J. Yin, C. D. Liang, H. Peng, L. H. Nie, and S. Z. Yao, "A study of a new TSM bio-mimetic sensor using a molecularly imprinted polymer coating and its application for the determination of nicotine in human serum and urine," *Bioelectrochem.*, vol. 53, pp. 141–148, 2001.
[13] R. Ganske, The use of the SAWS-Immuno-biosensor for detection of human interleukin-6 Axela Biosensors, 2006. [Online]. Available: http://www.atonomics.com
[14] E. Berkenpas, S. Bitla, P. Millard, and M. Pereira da Cunha, "Pure shear horizontal SAW biosensor on langasite," *IEEE Trans. Ultrason., Ferroelectr., Freq. Control*, vol. 51, no. 11, pp. 1404–1410, Nov. 2004.
[15] E. Berkenpas, P. Millard, and M. Pereira da Cunha, *Novel O157:H7 E.Coli Detector Utilizing a Langasite Surface Acoustic Wave Sensor*, pp. 1237–1240, 2005.
[16] E. Gizeli, F. Bender, A. Rasmusson, K. Saha, F. Josse, and R. Cernosek, "Sensitivity of the acoustic waveguide biosensor to protein binding as a function of the waveguide properties," *Biosensors Bioelectron.*, vol. 18, pp. 1399–1406, 2003.
[17] E. Gizeli, "Design considerations for the acoustic waveguide biosensor," *Smart. Mater. Struct.*, vol. 6, pp. 700–706, 1997.
[18] O. Tigli and M. Zaghloul, "A novel SAW device in CMOS: Design, modeling and fabrication," *IEEE Sensors J.*, vol. 7, no. 2, pp. 219–227, Feb. 2007.
[19] O. Tigli and M. Zaghloul, "Design and fabrication of a novel SAW biochemical sensor in CMOS," presented at the IEEE Sensors Conf., Special Session: CMOS Based Sensors, Irvine, CA, Oct. 2005, Invited talk.
[20] O. Tigli and M. Zaghloul, "Design, modeling and characterization of a novel circular surface acoustic wave device," *IEEE Sensors J.*, vol. 8, no. 11, pp. 1807–1815, Nov. 2008.
[21] A. F. Collings and F. Caruso, "Biosensors: Recent advances," *Rep. Prog. Phys.*, vol. 60, pp. 1397–1445, 1997.
[22] P. Sklada, "Piezoelectric quartz crystal sensors applied for bioanalytical assays and characterization of affinity interactions," *J. Braz. Chem. Soc.*, vol. 14-4, pp. 491–502, 2003.
[23] A. Janshoff and C. Steinem, "Sensors technology–applications–markets," in *Sensors Update*, H. Baltes, J. Hesse, and J. G. Korvink, Eds. Weinheim, Germany: Wiley-VCH, 2001, vol. 9, ch. 2, pp. 340–342.
[24] M. B. Cortie, *Properties and Potential Applications of Meso-Porous Gold*. Sydney, Australia: Univ. Technol. Sydney, Inst. Nanoscale Technol., 2003.
[25] E. Gizeli, "Design considerations for the acoustic waveguide biosensor," *Smart. Mater. Struct.*, vol. 6, pp. 700–706, 1997.
[26] J. Du, G. L. Harding, J. A. Ogilvy, P. R. Dencher, and M. Lake, "A study of love-wave acoustic sensors," *Sensors Actuators A*, vol. 56, pp. 211–219, 1996.
[27] E. Gizeli, A. Stevenson, N. J. Goddard, and C. R. Lowe, "A love plate biosensor utilizing a polymer layer," *Sensors Actuators B*, vol. 6, pp. 131–137, 1992.
[28] A. Kumar, "Biosensors based on piezoelectric detectors: Theory and application," *JOM-e*, vol. 52-10, 2000.
[29] K. Catt, G. W. Tregear, H. G. Burger, and G. Skermer, "Antibody-coated tube method for radioimmunoassay of human growth hormone," *Clin. Chim. Acta.*, vol. 27, pp. 267–279, 1970.
[30] N. J. Geddes, A. S. Martin, F. Caruso, R. S. Urquhart, D. N. Furlong, J. R. Sambles, K. A. Than, and J. A. Edgar, "Immobilization of IgG onto gold surfaces and its interaction with anti-IgG studied by surface plasmon resonance," *J. Immunol. Meth.*, vol. 175, no. 2, pp. 149–160, 1994.
[31] S. Tombelli, M. Minunni, and M. Mascini, "Piezoelectric biosensors: Strategies for coupling nucleic acids to piezoelectric devices," *Biosensors*, vol. 37-1, pp. 48–56, 2005.
[32] J. L. Bernstein, J. H. Godbold, G. Raptis, M. A. Watson, B. Levinson, S. A. Aaronson, and T. P. Fleming, "Identification of mammaglobin as a novel serum marker for breast cancer," *Clin. Cancer Res.*, vol. 11, pp. 6528–6535, 2005.
[33] P. N. Span, E. Waanders, P. Manders, J. J. M. Heuvel, J. A. Foekens, M. A. Watson, L. V. A. M. Beex, and F. C. G. J. Sweep, "Mammaglobin is associated with low-grade, steroid receptor-positive breast tumors from postmenopausal patients, and has independent prognostic value for relapse-free survival tim," *J. Clin. Oncol.*, vol. 22, pp. 691–698, 2004.
[34] K. Grunewald, M. Haun, M. Urbanek, M. Fiegl, E. Muller-Holzner, E. Gunsilius, M. Dunser, C. Marth, and G. Gastl, "Mammaglobin gene expression: A superior marker of breast cancer cells in peripheral blood in comparison to epidermal-growth-factor receptor and cytokeratin-19," *Lab. Invest.*, vol. 80, pp. 1071–1077, 2000.
[35] D. Ho, B. Chu, H. Lee, and C. D. Montemagno, "Directed protein orientation by site-specific labeling," in *Proc. IEEE Nanotechnology*, 2003, vol. 12-14, pp. 1084–1094.
[36] Cascade Microtech, Inc., Dec. 15, 2007. [Online]. Available: www.cascademicrotech.com
[37] *"User's Guide 8712ET and 8714ET RF Network Analyzers,"* Agilent Technologies, , 2007. [Online]. Available: www.agilent.com, 2000
[38] H. Liao, "Optical nonlinearity of nanocrystalline Au/ZnO composite films," *Opt. Lett.*, vol. 28, no. 19, pp. 1790–1792, 2003.
[39] D. D. Stubbs, S.-H. Lee, and W. D. Hunt, "Molecular recognition for electronic noses using surface acoustic wave immunoassay sensors," *IEEE Sensors J.*, vol. 2, no. 4, pp. 294–300, Aug. 2002.
[40] G. McHale, M. I. Newton, and F. Martin, "Theoretical mass sensitivity of love wave and layer guided acoustic plate mode sensors," *J. Appl. Phys.*, vol. 91, no. 12, pp. 9701–9710.

Onur Tigli (M'08) was born in Istanbul, Turkey, in 1979. He received the B.S. degree (Hons.) in electrical and electronics engineering from the Middle East Technical University (METU), Ankara, Turkey, in 2000, and the M.S. and D.Sc. degrees in computer engineering from The George Washington University (GWU), Washington, DC, in 2002 and 2007, respectively.

During his graduate studies, he worked for the National Institute of Standards and Technology (NIST) Semiconductor Electronics Division, Naval Research Lab (NRL) Materials Science and Technology Division, and completed projects on areas of system-on-a-chip, application-specific integrated-circuit field-programmable gate-array (ASIC/FPGA) design, chemical sensors, and microelectromechanical-systems (MEMS) fabrication techniques. Currently, he is an Assistant Professor of Electrical Engineering at Washington State University Vancouver. His current research deals with the development of zinc–oxide nanowire-based biosensors for single molecule detection of cancer biomarkers as well as complementary metal–oxide semiconductor-compatible nano/microfabrication techniques, finite-element method modeling for nanoelectromechanical systems and acoustic MEMS, and evolvable hardware employing digital ASIC/FPGA design techniques. He has three provisional patent applications pending for the development of "CMOS-SAW based biochemical sensor with temperature control," "A novel circular SAW device in CMOS," and "Multiplex biosensor for cancer biomarker detection."

Dr. Tigli has held several teaching positions at GWU since 2002, for which he received the Philip Amsterdam excellence in teaching award in 2006. His dissertation "Novel SAW devices in CMOS for biosensor applications: Design, modeling, fabrication and characterization" was selected as the official nominee of GWU for the 2008 CGS/UMI Distinguished Dissertation Award.

Louis Bivona was born in Baltimore, MD, in 1984. He received the B.S. degree in biochemistry from the University of Maryland, College Park, in 2006 and the M.S. degree in biochemistry from The George Washington University, Washington, DC.

He worked in the laboratory of Dr. Patricia Berg, where his main research focus was developing a blood screen as an early detection tool for breast cancer. He currently performs research at the National Institutes of Health, Rockville, MD, and is with the Laboratory of Immunogenetics, developing novel techniques aiding in recombinant protein expression.

Patricia Berg received the B.A. degee in mathematics from the University of Chicago, Chicago, IL, and the Ph.D. degree in microbiology from the Illinois Institute of Technology, Chicago.

Currently, she is a Professor in the Department of Biochemistry and Molecular Biology at the George Washington University Medical Center. Her basic molecular biology/translational laboratory is focused on the study of a gene she discovered and cloned, called BP1. Her laboratory has shown that BP1 is activated in 80% of invasive ductal breast tumors, 70% of prostate tumors, and 63% of acute myeloid leukemias. In breast cancer, the BP1 expression is associated with aggressive tumors and progression. Her laboratory is studying the molecular pathways regulated by BP1 in tumor cells and, on the clinical side, is testing possible suppressors. In addition, the development of a blood test is underway, making it important to develop assays for sensitive detection of biomolecules in blood.

Mona E. Zaghloul (M'81–SM'85–F'96) received the B.S. degree from Cairo University, Egypt, in 1965, and the Masters degree in science, the Masters degree in math, and the Ph.D. degree from the University of Waterloo, Waterloo, ON, Canada, in 1970, 1971, and 1975, respectively.

Currently, she is a Professor of Electrical and Computer Engineering at the George Washington University, Washington, DC, where she is also Director for the Institute for MEMS and VLSI Technology. She has published more than 270 technical papers in the general areas of circuits and systems, microelectronics system design, very-large-scale integrated (VLSI) circuits design, sensors design, and microelectromechanical systems. She has also contributed to several books. Her main research interests are in the areas of analog design of VLSI circuits, design, and implementation of microelectromechanical systems (MEMS) with applications to radio frequency (RF)-MEMS, and biosensors.